Ece Bayrak, Burak Ozcan and Cevat Erisken*

Processing of polycaprolactone and hydroxyapatite to fabricate graded electrospun composites for tendon-bone interface regeneration

DOI 10.1515/polyeng-2016-0017
Received January 15, 2016; accepted March 23, 2016; previously published online May 3, 2016

Abstract: The process of electrospinning is utilized with different approaches including conventional electrospinning, extrusion electrospinning, and electroblowing to form nanofibrous meshes and composites. Here, we report on the quality and properties of spatially graded polycaprolactone (PCL) and nano-hydroxyapatite (nHA) composite meshes fabricated with multiple-spinneret electrospinning. The composite meshes were characterized in terms of the amount of spatially allocated nHA concentration across the mesh, fiber diameter, porosity, pore size, and hydrophilicity of meshes. Results show that linearly and continuously varying nHA concentration distribution, i.e. graded structure, can be accomplished across the mesh thickness using multiple-spinneret electrospinning, which is in accordance with the change of mineral concentration observed in native tendon-bone interface. Furthermore, incorporation of nanoparticles into nanofibers led to increased fiber diameter as depicted by a shift in fiber diameter distribution, a significant increase in mean fiber diameter from 361±9 nm to 459±21 nm, and an increase in contact angle from 120.01±2.77° to 115.24±1.17°. These findings suggest that the composite meshes formed in this study could serve as model systems to be used as scaffolds in tendon-bone tissue engineering application in particular, and for other tissue-tissue interfaces in a broader context.

Keywords: grading; hydroxyapatite; interface; multiple-spinneret electrospinning; polycaprolactone; regeneration; tissue engineering.

***Corresponding author: Cevat Erisken,** Department of Biomedical Engineering, TOBB University of Economics and Technology, Sogutozu Avenue No 43, Sogutozu, Ankara 06560, Turkey, e-mail: cerisken@etu.edu.tr
Ece Bayrak and Burak Ozcan: Department of Biomedical Engineering, TOBB University of Economics and Technology, Sogutozu Avenue No 43, Sogutozu, Ankara 06560, Turkey

1 Introduction

Electrospinning has been utilized for polymer processing to generate fibers, nanofibers, and fibrous composites since the 1930s [1, 2]. The process typically involves feeding a conductive polymeric solution or melt in a reservoir, with a spinneret on one side and a collector on the other, and forming fibers as a result of electrical potential difference, which aims at overcoming the surface tension of the polymer droplet and forcing the fiber jet to travel downstream to reduce the jet diameter.

Currently, the process is utilized with different approaches such as conventional electrospinning, extrusion electrospinning, electroblowing, etc. yet, all are based on the same principles of balance of mass, momentum and electric charges [3]. Among these approaches, conventional electrospinning, the most widely used approach, involves loading the ingredients into a reservoir and forcing the contents out for the polymer to travel towards a collecting surface as a result of potential difference [4]. Extrusion electrospinning, by contrast, is a hybrid process consisting of an extruder integrated with the electrospinning process [5]. Presence of the injection ports and other feed ports enables the feeding of various liquid and solid ingredients/additives simultaneously. The ability to introduce ingredients of multiple formulations in a time-dependent fashion during the process is a major advantage of extrusion electrospinning. This characteristic readily allows for the manufacture of spatially graded electrospun membranes. In the electroblowing technique, air blowing and electrospinning are combined to form a hybrid process [6, 7]. The polymer jet leaving the spinneret is accompanied by a gas jet surrounding the spinneret, mainly to increase the production capacity and to control the jet direction.

In the context of regenerative engineering, the process of electrospinning finds application for a variety of tissues including bone, cartilage, tendon, ligament, and skin [8]. More importantly, this process also allows us to fabricate

spatially graded structures to be particularly utilized for the regeneration/repair of tissue-tissue interfaces, which possess location-dependent changes, i.e. gradients, in terms of composition of ingredients and structural properties. Such tissue interfaces may include, but are not limited to, cartilage-bone, tendon-bone, ligament-bone, and tendon-muscle junctions.

Experimental research in this field demonstrates that many polymeric biomaterials are suitable to process with electrospinning. In this regard, poly(D,L-lactide-co-glycolide), and polycaprolactone (PCL) are commonly electrospun for tissue engineering applications mainly because they are approved by the Food and Drug Administration, USA, to be used as materials of construction for a variety of biomedical devices. We and others previously utilized conventional electrospinning to form poly(D,L-lactide-co-glycolide) nanofiber meshes with controlled fiber diameters, and evaluated their performance using cells from different sources including tendon fibroblasts [9] and NIH 3T3 fibroblasts [10]. Our group also electrospun PCL and beta tricalcium phosphate (beta-TCP) nanoparticles to generate spatially graded composite meshes for osteochondral (cartilage-bone interface) tissue regeneration applications [11]. Test results confirmed their *in vitro* cytocompatibility and native-like tissue formation with adipose derived stem cells [12].

The spatial grading can be introduced into the electrospun meshes by different process modifications. In extrusion-electrospinning [5], each and every single raw material is fed to the extruder where the mixing and pressurization takes place with the aid of rotating screws. The electric field is generated between the collecting surface and the spinneret attached to the die. The gradient is achieved by controlling the feed rate of each component. Another modification is based on pumping the solution and suspension from two separate syringes and mixing them into a single channel to which the spinneret is attached and potential difference is applied [13]. In this process, the gradient is formed by adjusting the pumping speeds for the syringes. A third modification would be running the two syringes either in parallel or in opposing directions, i.e. multiple-spinneret electrospinning. Both modifications were previously tested to form composite meshes. For example, opposing syringe case was employed to form fibrous scaffolds where each syringe contained protease-degradable and non-degradable methacrylated peptide hyaluronic acid, with no gradient introduced [14]. In another case, a gradient of hydroxyapatite mineral nanoparticles was generated across a blend of electrospun PCL and poly(ester urethane) urea mesh thickness, and it was used to test its suitability for ligament-bone interface applications [15]. In this earlier study, the presence of mineral particles, but not the actual concentration loaded at 3% by weight, was verified with X-ray diffraction and energy-dispersive spectroscopy, and functionality was tested with gradients of mechanical properties, as well as the response of the MC3T3-E1 cell line. Probably because this 3% concentration of nano-hydroxyapatite (nHA) particles was not high enough to represent the concentration at the ligament-bone interface, they also deposited additional minerals by dipping the samples into 5x simulated body fluid.

In this study, we aim at: (i) fabricating continuously graded PCL-nHA composite meshes with multiple-spinneret electrospinning using two opposing syringes, with nHA concentration loading level of 20% by weight; (ii) measuring the amount of spatially allocated nHA concentration gradients across the mesh using thermogravimetric analysis; and (iii) testing the effect of mineral loading on the pore size, hydrophilicity, and fiber diameter of meshes. We chose PCL mainly because it is approved by the Food and Drug Administration, and is suitable for tendon tissue engineering [16]. To form composite meshes, we used nHA because it is the main mineral ingredient in the native bone tissue [17]. Electrospinning these two components, namely PCL and nHA, simultaneously in a feed rate controlled manner would generate spatially graded PCL-nHA composite meshes, which would be very suitable for tendon-bone interface tissue engineering applications. It is accepted and demonstrated [18] that the tendon-bone interface is characterized by continuously changing mineral concentrations across the interface. Therefore, the composite mesh fabricated here could mimic this interface and be potentially utilized for its regeneration/repair.

Design and processing of biomimetic scaffolds to be utilized in interface tissue engineering is a challenge, because interfaces possess complex structures with smooth transitions in properties and functions at relatively small distances. For example, an investigation on the supraspinatus tendon-to-bone insertion of Fisher Rat demonstrated that change in mineral content occurs within ~120 μm resolution [18]. Since an abrupt change in material properties between two homogeneous materials generally leads to mechanical failure due to high stress concentrations accumulated at the interface, fabrication of devices with gradients in properties at physiological resolution is a requirement for better mimicking the structures and functions of native tissues. In this context, prior attempts to fabricate scaffolds for tendon-bone tissue engineering involved either an irrelevant scale for gradient [19] or biphasic (two-layer, mineralized, and

unmineralized) approach for the change of concentration of ingredients [20]. However, designing and fabricating functionally graded biomaterials at physiologically-relevant resolutions to be utilized in the engineering/regeneration of interfaces is needed, and this study aimed at meeting this need.

It is expected that the composite meshes formed in this study will serve as model systems to be used as scaffolds in tendon-bone tissue engineering application. In addition, this study will also contribute to the pool of research performed with different electrospinning approaches, which can then be used to compare the efficacy of these approaches in the generation of graded scaffolds. In a much broader sense, this study will generate data that could be useful for other interface tissue engineering applications in addition to tendon-bone interface. Our future studies will include incorporation of growth factors into the composite mesh formed here to stimulate differentiation of stem cells into tendon and bone lineages across the mesh thickness and test it *in vitro*. The ultimate goal is to fabricate a clinically feasible graded construct.

2 Materials and methods

2.1 Materials and instruments

All materials including PCL (Cat# 440744), dichloromethane (Cat# 676853), N,N-dimethylformamide (DMF, Cat# D158550), and hydroxyapatite (nHA, Cat# 677418) were purchased from Sigma-Aldrich, St Louis, MO, USA. The sonicator (Cat#142-1130) was obtained from Bandelin, Berlin, Germany. The vortex mixer (Model VX14018092) is a product of Bio-Active, Bangkok, Thailand. Syringe pumps (Model NE-300) were from New Era Pump Systems, Farmingdale, NY, USA. The thermogravimetric analyzer (TGA-Q50) was procured from TA Instruments, New Castle, DE, USA. The scanning electron microscope (Quanta 200) is from FEI, Hillsboro, OR, USA. The optical tensiometer (Model T200KSV) was purchased from Biolin, Stockholm, Sweden. ImageJ software was available from National Institutes of Health, Bethesda, MD, USA.

2.2 Preparation of PCL solution and hydroxyapatite suspension

The nanofiber meshes were fabricated by electrospinning. Briefly, in order to make PCL solution, PCL with a number average molecular weight of 80,000 was dissolved in a mixture of dichloromethane and DMF at a ratio of 20/100 (g/ml). The ratio of dichloromethane/DMF was set to 2/3 by volume. To make the hydroxyapatite suspension, nHA particles were dispersed in 200 µl of DMF using a sonicator, and then added to PCL solution at an nHA/PCL ratio of 0.2/1 (mg/mg) such that the highest nHA concentration in the mesh will be 20% by weight on the nHA rich side. The solution and suspension were homogenized using a vortex mixer for 5 h.

2.3 Multiple electrospinning with opposing spinnerets

PCL solution and nHA suspension were transferred to syringes attached with needles of ~0.9 mm inner diameter. The syringes were then loaded to two separate pumps, which were also stationed in opposing directions across a cylindrical mandrel rotating at ~7.5 m/s (Figure 1). The distance between the tip of the needles and the rotating mandrel was kept at 13 cm. A potential difference of 8–10 kV was applied during the process. The pump speeds were incrementally changed at 0.14 ml every hour so as to decrease the flow rate of PCL solution from 1.0 ml/h to 0.0 ml/h, and increase that of nHA suspension from 0.0 ml/h to 1.0 ml/h, the total flow rate being 1.0 ml/h at all times (See Table 1). The process took approximately 8 h to complete.

2.4 Mesh characterization:

The weight fraction of nHA contained in electrospun PCL-nHA meshes was validated by using a thermogravimetric analysis apparatus upon heating from 25°C to 660°C at 40°C/min under N_2.

The porosity of the electrospun meshes was determined by using their apparent (bulk) densities (n=3) using the equation:

$$\varepsilon = 1 - \rho_a / \rho_t$$

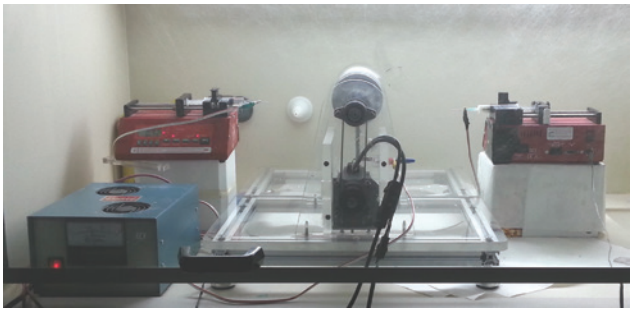

Figure 1: Picture of the multiple-spinneret electrospinning set up.

Table 1: Flow rates of the fluids in the two-opposing syringes during the process.

PCL-only (ml/h)	PCL-nHA (ml/h)	Total flow rate (ml/h)
1.00	0.00	1.00
0.86	0.14	1.00
0.72	0.28	1.00
0.58	0.42	1.00
0.44	0.56	1.00
0.30	0.70	1.00
0.16	0.84	1.00
0.00	1.00	1.00

nHA, Nano-hydroxyapatite; PCL, polycaprolactone.

where ρ_t is the true density of the material, ρ_a is the apparent density, and ε is the porosity. Apparent density was calculated by dividing the weight of cuboid samples by the volume, which was calculated using the dimensions of the samples.

Pore size was determined by measuring the longest and shortest distances of irregularly shaped pore openings between fibers using micrographs generated by scanning electron microscopy (SEM, n=3/group). An ImageJ software was utilized for measurements. Approximately 30 values were recorded for each SEM image and diameter distribution was determined based on a bin range. The values for three samples were then averaged for each increment to obtain a mean pore size distribution.

The diameter, shape, and surface properties of the electrospun fibers were evaluated using SEM micrographs. Mineral presence was verified quantitatively by spectrums from the meshes. Fiber diameters were measured with ImageJ from the SEM images (n=3/group). Briefly, each image was segmented with five vertical lines of equal spacing, and fibers intersecting with the verticals were marked. The diameters of these fibers were measured by ImageJ, and a mean fiber diameter was calculated (averaging n=40 fibers/image).

The contact angles of the PCL-rich and nHA-rich surfaces of composite meshes were measured using a theta optical tensiometer in conjunction with the sessile drop method. Specifically, 2 µl of deionized water droplet was placed on the surface of meshes and imaged within 5 s. The contact angles were then measured using ImageJ software (n=3/group).

2.5 Statistics

The pore size, contact angle, and diameter of the PCL-rich and nHA-rich sides of the meshes were evaluated using student's t test. The p levels at which differences between groups are considered statistically significant is taken as 0.05 or less.

3 Results and discussion

3.1 Weight distribution of nHA particles

The electrospinning process generated meshes with thickness of 220.2±3.2 µm on average (n=3), which can be tailored by controlling the process time. In this study, the process was ceased after approximately 8 h, because the thickness obtained within this period would be appropriate for tendon-bone regeneration applications. Tendon-bone interface thickness in native tissue is reported to change between 100–200 µm [18]. The presence of nHA mineral particles within the entire mesh was determined from samples obtained from eight different and equally spaced locations. This enabled us to evaluate the spatial distribution of nHA particles as a function of mesh thickness (Figure 2). As seen in Figure 2, the spatial inclusion of nHA particles into the mesh exhibits a linear distribution. This is the result of linearly varied flow rates of mesh ingredients, namely the PCL solution and nHA suspension.

The highest nHA concentration in the mesh was determined as 16.02±0.41% as compared to 20% loaded actually. The mismatch between the actually loaded nHA and experimentally measured nHA concentrations can be explained by the weakness of the conventional electrospinning process for processing particles, especially

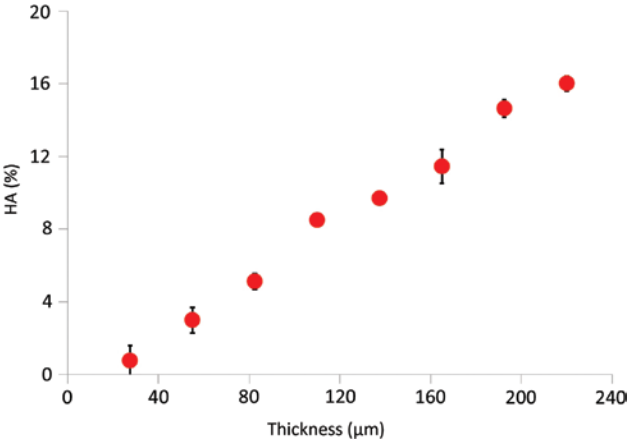

Figure 2: Spatially changing composition of nano-hydroxyapatite (nHA) particles across mesh thickness. Error bars represent standard deviations (STDs).

those with high densities. The process takes about 8 h to form a mesh thickness of ~220 μm, which is long enough for some of the mineral particles suspended in the syringe to settle down due to significant density difference (nHA has a density of ~3.16 g/ml while PCL has a density of ~1.45 g/ml). We earlier ran a suspension of beta-TCP through an extrusion electrospinning process and obtained a concentration of 35±1.5% versus 35% loaded actually [5]. Since the extruder continuously disperses and distributes the particles during the process, the closeness of actual and experimental loading levels is not surprising. Overall, Figure 2 clearly demonstrates that the linearly and continuously varying nHA concentration was accomplished across the mesh thickness, which is in accordance with the change of mineral concentration observed across the native tendon-bone interface [18].

3.2 Fiber diameter and surface properties

The SEM micrographs taken from PCL-rich and nHA-rich surfaces of the meshes are depicted in Figure 3. The nanofibers generated on the PCL-rich side of the mesh look smooth and uniform in diameter. Similarly, the nanofibers collected on the nHA-rich side also look uniform in diameter, yet possess irregular protruded morphology due to incorporation of nanoparticles (Figure 3B, white arrows). It is seen that nHA particulates were either embedded into nanofibers or positioned on the fiber surfaces. Also present are the particle agglomerates with diameters larger than those of nanofibers. The presence of these nHA agglomerates in or on the surface of the fibers demonstrates that nanoparticles processed with conventional electrospinning are prone to agglomerations likely due to electrostatic forces

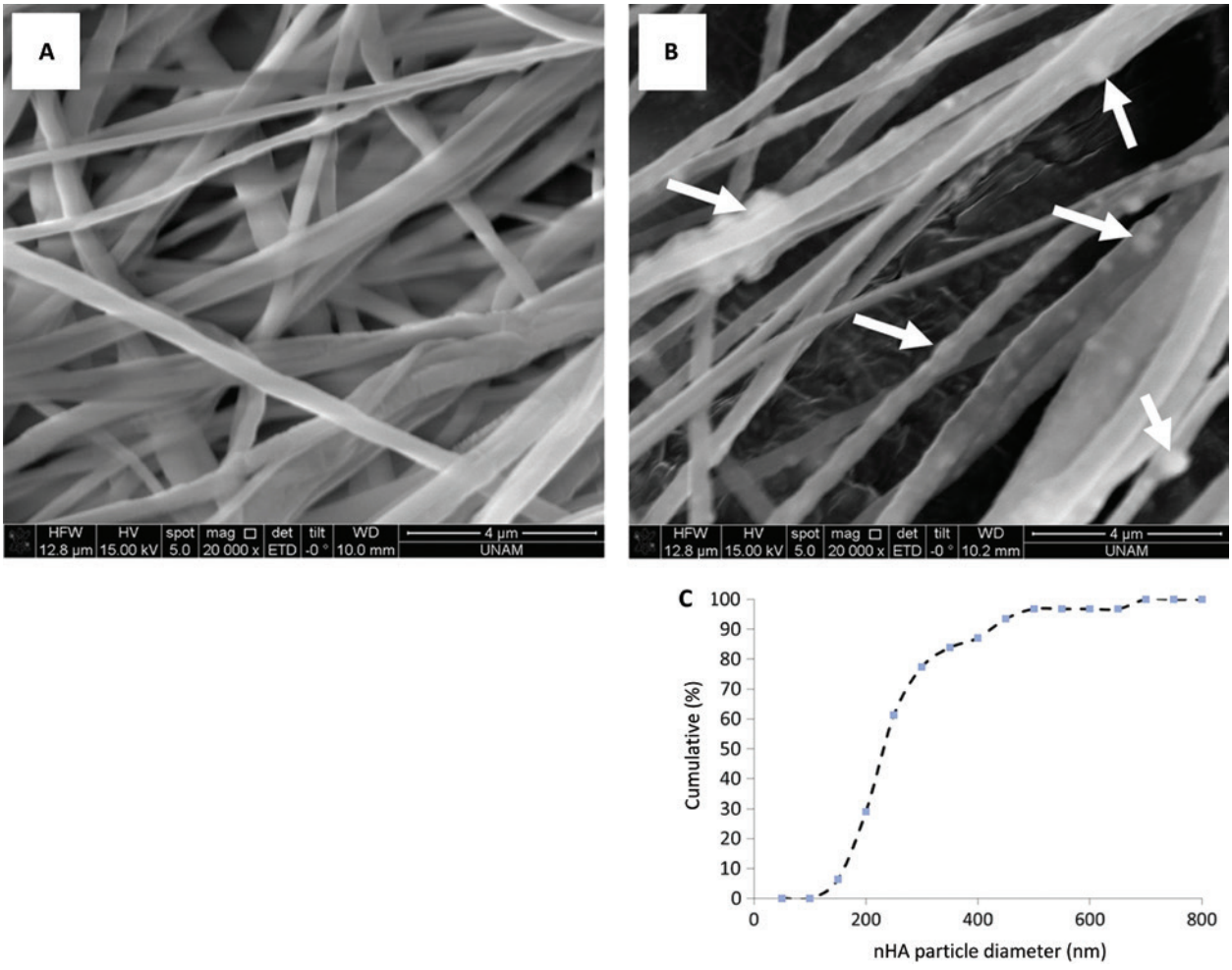

Figure 3: Representative scanning electron microscopy (SEM) micrographs taken from (A) polycaprolactone (PCL)-rich and (B) nano-hydroxyapatite (nHA)-rich surfaces of the spatially graded meshes, and (C) diameter distribution of nHA particulates appeared on micrographs. White arrows in B indicate nHA particulates embedded into nanofibers. Scale bars are 4 μm.

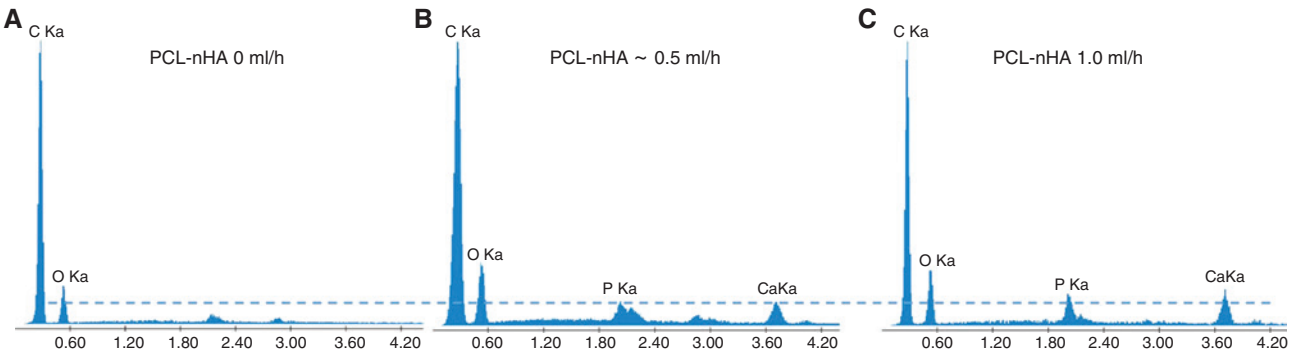

Figure 4: Energy dispersive spectroscopy (EDS) spectrum of polycaprolactone (PCL)-only and PCL-nano-hydroxyapatite (nHA) meshes at different flow rates corresponding to different nHA concentrations.

generated before and during mixing. Although the nHA suspension was sonicated prior to electrospinning, this intervention seems to be inadequate. A further study was performed to see if these particulates are agglomerates or individual nHA nanoparticles by measuring the size of white marks, presumably representing nHA minerals, observed in SEM micrographs. The findings, shown in Figure 3C, demonstrate that only around 30% of the particles are in the range specified by the manufacturer (particle size <200 nm). Therefore, it is possible to claim that the conventional electrospinning process is unable to break the agglomerates efficiently, which are formed before or during the process. Unlike what was observed here, earlier reports on the processing of nanoparticles using the extrusion electrospinning process suggests that nanoparticles can be efficiently dispersed and distributed during processing, thus preventing formation of large agglomerates [5]. Figure 4 also verifies the presence of the nHA particles as indicated by Ca and P peaks and their increasing intensity with increasing nHA content.

Incorporation of nanoparticles into nanofibers led to increased fiber diameter as depicted by a shift in fiber diameter distribution (Figure 5A and B), as well as a significant increase in mean diameter determined statistically (Figure 5C). The mean fiber diameters of the PCL-rich and nHA-rich side of the meshes were calculated as 361±9 nm and 459±21 nm, respectively. A similar effect of nanoparticle inclusion on fiber diameter was also reported by other investigators [5, 21]. The reason for increased fiber diameter could be partly explained by the presence of agglomerates of nHA. It is known that polymer jet diameter goes down as it travels from the spinneret tip to the collecting surface, defined by a draw-down ratio, and the diameter of the jet at the time it hits the surface defines the ultimate fiber diameter. In the absence of particles, this reduction in diameter should follow a defined smooth path, provided that the material, process and ambient conditions remain controlled. In the presence of particles, however, the continuous decrease in diameter may be disrupted at some point so as to disturb the process either temporarily or permanently. Since it is extremely difficult to have perfectly dispersed nanoparticles in a suspension, especially in processes like electrospinning, to answer the question whether we would have increased fiber diameter in the absence of agglomerates or not should require carefully designed experiments.

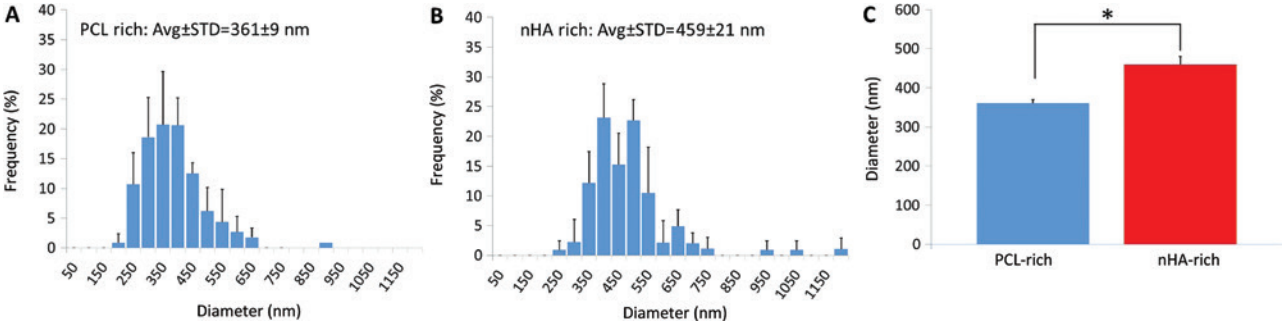

Figure 5: Fiber diameter distribution of meshes measured from (A) polycaprolactone (PCL)-rich and (B) nano-hydroxyapatite (nHA)-rich surfaces, and (C) comparison of their mean diameter. *indicates significant difference between groups ($p<0.05$).

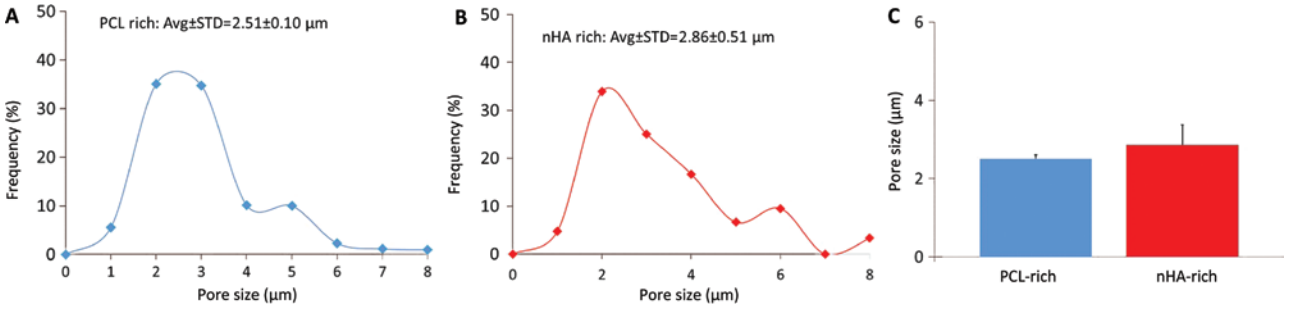

Figure 6: Pore size distribution of (A) polycaprolactone (PCL)-rich side, (B) nano-hydroxyapatite (nHA)-rich side of the meshes, and (C) mean pore sizes. No significant difference exists between the groups, $p>0.05$. Error bars represent standard deviations (STDs).

3.3 Porosity and pore size

Porosity of the PCL-nHA spatially graded meshes was determined to be 98.55±0.01%. The electrospinning process is known to generate highly porous, interconnected meshes, and is therefore preferred for a wide range of tissue engineering applications. A study performed earlier using the extrusion electrospinning process generated a porosity value of 87±2% for PCL-beta-TCP meshes containing a gradient of 35%, by weight, beta-TCP across the mesh. Overall, porosity of our mesh fabricated here seems appropriate for cartilage tissue engineering [22] as well as cartilage-bone interface applications [11].

Pore size and size distribution were reported based on the SEM micrographs taken from the PCL-rich and nHA-rich sides of the meshes (Figure 6). Clearly, there is no significant effect of nHA addition on the mean pore size and pore size distribution (Figure 6A and B). As seen in Figure 6A and B, the mean pore size of meshes was calculated as 2.51±0.10 µm for PCL-rich surface and 2.86±0.51 µm for nHA-rich surface. In the context of tissue engineering applications of these meshes, investigators have found limited penetration of the cells into the nanofibrous structures, because the pore size generated is generally much smaller than the actual cell size (may vary from roughly 5 µm to 30 µm depending on the cell type). Our findings also verify such claims. Prior research demonstrates that the major determinants of pore size are the fiber diameter and porosity, and that it may not always be possible to control all simultaneously. In this regard, Eichhorn and Sampson [23] performed a parametric study to mathematically model the relation between pore size, porosity, and diameter. They found that there is a positive relation between fiber diameter and pore diameter. Obviously, we would not like to increase fiber diameter at the expense of pore diameter due to strong biomimicry of nanofibers. In such cases, a straight forward approach to increase pore size could be to blend the main polymer material with water soluble polymers and dissolve them post fabrication to generate additional volumes [24].

3.4 Contact angle

The mean contact angles of the PCL-rich and nHA-rich surfaces of the composite mesh are given in Figure 7. Apparently, the incorporation of nHA ceramic nanoparticles into PCL decreases the contact angle from 120.01±2.77° to 115.24±1.17° upon increase of surface energy, which is also consistent with earlier studies [5, 25]. In addition, since PCL is a hydrophobic polymer and nHA is relatively hydrophilic, addition of nHA particles into PCL should result in reduced contact angle, which was the case in this study.

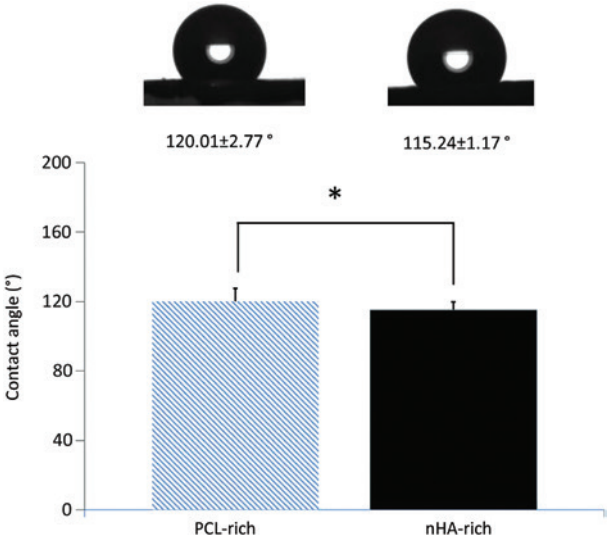

Figure 7: Contact angles of polycaprolactone (PCL)-rich and nano-hydroxyapatite (nHA)-rich surfaces of composite meshes. Representative images of DI water droplets on mesh surfaces. *indicates significant difference between groups ($p<0.05$).

4 Conclusions

In this study, we investigated the quality and properties of spatially graded PCL and nHA composite meshes fabricated with multiple-spinneret electrospinning. Our findings demonstrated that controlled compositional gradients of nHA can be accomplished across the thickness of PCL mesh. Furthermore, a difference in terms of physical properties including fiber diameter and contact angle could be created across the composite mesh with mineral incorporation. These findings suggest that the composite meshes formed in this study could serve as model systems to be used as scaffolds in tendon-bone tissue engineering application in particular, and for other tissue-tissue interfaces in a broader context. We plan to use the results of this study in our future works that will include incorporation of growth factors and testing the cytotoxicity of the composite meshes, as well as testing their capacity to stimulate differentiation of stem cells into tendon and bone lineages across the mesh thickness.

Acknowledgments: We are grateful to Dr. Dilhan Kalyon for providing the facilities of Highly Filled Materials Institute, Hoboken, NJ, for thermogravimetric characterizations. We thank Dr. Mehmet Mutlu, Dr. Fatih Büyükserin, and Ms. Sevde Altuntas, TOBB University of Economics and Technology, Turkey, for their technical support. We also thank Ms. Gonca Bilge, for her help with contact angle measurements. The authors gratefully acknowledge funding support from the Scientific and Technological Research Council of Turkey (Project no. 115C001).

Conflict of interest statement: The authors deny any conflicts of interest related to this study.

References

[1] Formhals A, US Patent 1934.
[2] Doshi J, Reneker DH. *J. Electrost.* 1995, 35, 151–160.
[3] Fridrikh SV, Yu JH, Brenner MP, Rutledge GC. *Phys. Rev. Lett.* 2003, 90, 144502.
[4] Reneker DH, Chun I. *Nanotechnology* 1996, 7, 216–223.
[5] Erisken C, Kalyon DM, Wang H. *Nanotechnology* 2008, 19, 165302.
[6] Um IC, Fang D, Hsiao BS, Okamoto A, Chu B. *Biomacromolecules* 2004, 5, 1428–1436.
[7] Kong CS, Yoo WS, Lee KY, Kim HS. *J. Mater. Sci.* 2009, 44, 110–1112.
[8] Khorshidi S, Solouk A, Mirzadeh H, Mazinani S, Lagaron JM, Sharifi S, Ramakrishna S. *J. Tissue Eng. Regener. Med.* doi: 10.1002/term.1978.
[9] Erisken C, Zhang X, Moffat KL, Levine WN, Lu HH. *Tissue Eng., Part A* 2013, 19, 519–528.
[10] Bashur CA, Dahlgren LA, Goldstein AS. *Biomaterials* 2006, 27, 5681–5688.
[11] Erisken C, Kalyon DM, Wang H. *Biomaterials* 2008 29, 4065–4073.
[12] Erisken C, Kalyon DM, Wang H, Ornek-Ballancob C, Xu J. *Tissue Eng., Part A* 2011, 17, 1239–1252.
[13] Sundararaghavan HG, Burdick JA. *Biomacromolecules* 2011, 12, 2344–2350.
[14] Wade RJ, Bassin EJ, Rodell CB, Burdick JA. *Nat. Commun*. 2015, 6, 6639.
[15] Samavedi S, Olsen HC, Guelcher SA, Goldstein AS, Whittington R. *Acta Biomater.* 2011, 7, 4131–4138.
[16] Bosworth LA, Rathbone SR, Bradley RS, Cartmell SH. *J. Mech. Behav. Biomed. Mater.* 2014, 39, 175–183.
[17] Clarke B. *Clin. J. Am. Soc. Nephrol.* 2008, 3, 131–139.
[18] Genin GM, Kent A, Birman V, Wopenka B, Pasteris JD, Marquez PJ, Thomopoulos S. *Biophys. J.* 2009, 97, 976–985.
[19] Li X, Xie J, Lipner J, Yuan X, Thomopoulos S, Xia Y. *Nano. Lett.* 2009, 9, 2763–2768.
[20] Zhang X, Caldwell J-M, Easley JT, Hackett E, Doty S, Levine WN, Guo XA, Lu HH. Transactions of Orthopedic Research Society. 2014.
[21] Wutticharoenmongkol P, Sanchavanakit N, Pavasant P, Supaphol P. *Macromol. Biosci.* 2006, 6, 70–77.
[22] Setton LA, Elliott DM, Mow VC. *Osteoarthr. Cartil.* 1999, 7, 2–14.
[23] Eichhorn SJ, Sampson WW. *J. R. Soc. Interface* 2005, 2, 309–318.
[24] Baker BM, Gee AO, Metter RB, Nathan AS, Marklein RA, Burdick JA, Mauck L. *Biomaterials* 2008, 29, 2348–2358.
[25] Liao HT, Chen YY, Lai YT, Hsieh MF, Jiang CP. *Biomed. Res. Int.* 2014, 2014, 321549.